Journal of Process Control 24 (2014) 448–462

Contents lists available at ScienceDirect

Journal of Process Control

journal homepage: www.elsevier.com/locate/jprocont

Economic model predictive control of parabolic PDE systems: Addressing state estimation and computational efficiency

Liangfeng Lao [a], Matthew Ellis [a], Panagiotis D. Christofides [a,b,*]

[a] Department of Chemical and Biomolecular Engineering, University of California, Los Angeles, CA 90095-1592, USA
[b] Department of Electrical Engineering, University of California, Los Angeles, CA 90095-1592, USA

ARTICLE INFO

Article history:
Received 22 October 2013
Received in revised form 12 January 2014
Accepted 13 January 2014
Available online 21 February 2014

Keywords:
Model predictive control
Process economics
Partial differential equations (PDEs)
Process control
Transport-reaction processes

ABSTRACT

In a previous work [20], an economic model predictive control (EMPC) system for parabolic partial differential equation (PDE) systems was proposed. Through operating the PDE system in a time-varying fashion, the EMPC system demonstrated improved economic performance over steady-state operation. The EMPC system assumed the knowledge of the complete state spatial profile at each sampling period. From a practical point of view, measurements of the state variables are typically only available at a finite number of spatial positions. Additionally, the basis functions used to construct a reduced-order model (ROM) for the EMPC system were derived using analytical sinusoidal/cosinusoidal eigenfunctions. However, constructing a ROM on the basis of historical data-based empirical eigenfunctions by applying Karhunen-Loève expansion may be more computationally efficient. To address these issues, several EMPC systems are formulated for both output feedback implementation and with ROMs based on analytical sinusoidal/cosinusoidal eigenfunctions and empirical eigenfunctions. The EMPC systems are evaluated using a non-isothermal tubular reactor example, described by two nonlinear parabolic PDEs, where a second-order reaction takes place. The model accuracy, computational time, input and state constraint satisfaction, and closed-loop economic performance of the closed-loop tubular reactor under the different EMPC systems are compared.

1. Introduction

Model predictive control (MPC) is a popular optimal control technique that has gained widespread popularity within the process control industries. In the past decade, significant work has been done on MPC of partial differential equation (PDE) systems (e.g., [8–10,12,19,21,24,25]). To guide the PDE system to the desired steady-state profile, conventional MPC systems are formulated with the sum of squared differences between the state and inputs from their corresponding steady-state values. More recently, economic model predictive control (EMPC) formulated with a general cost function accounting directly for the process economics, which operates systems in a dynamically optimal fashion, has been proposed for systems described by ordinary differential equations (ODEs) (e.g., [7,13,17,16,18]).

The significant challenge to applying the proposed EMPC systems directly to PDE systems is deriving a finite-dimensional ordinary differential equation (ODE) in time approximation of the PDE model. Specifically, the finite-dimensional model must accurately predict the spatiotemporal evolution of the system, while, be of sufficiently low order for computational efficiency. To produce a model-based control scheme for parabolic PDEs, Galerkin's method based on either analytical or empirical basis functions is typically applied to the PDE model. In addition, utilizing approximate inertial manifolds (AIMs) (e.g., [6,11]), a system of finite-dimensional ODEs that accurately describe the dynamics of the dominant (slow) modes of the PDE system is derived for the synthesis of low-order controllers (e.g., [2] and the book [5]). Order reduction using Galerkin's method and analytical eigenfunctions was employed in [20] where we proposed an EMPC scheme for parabolic PDE systems.

While, the EMPC system of [20] demonstrated improved closed-loop economics (greater production rate of the desired product over steady-state operation), the EMPC system assumed the knowledge of the complete state spatial profile at each sampling period. In practice, however, measurements of the PDE system may only be available at a finite number of points. Therefore, the formulation of an output feedback EMPC for parabolic PDE systems based on measurements at a finite number of points should be considered.

Additionally, the EMPC systems presented in [20] were developed on the basis of low-order and high-order nonlinear ordinary differential equation (ODE) models derived through Galerkin's

* Corresponding author at: Department of Chemical and Biomolecular Engineering, University of California, Los Angeles, CA 90095-1592, USA. Tel.: +1 310 794 1015; fax: +1 310 206 4107.
E-mail address: pdc@seas.ucla.edu (P.D. Christofides).

0959-1524/$ – see front matter © 2014 Elsevier Ltd. All rights reserved.
http://dx.doi.org/10.1016/j.jprocont.2014.01.007

method using analytical basis functions. Considering the possible limitation for using analytical basis functions and to improve the ROM accuracy, empirical eigenfunctions as the basis functions for the Galerkin's method may be considered. The empirical eigenfunctions may be constructed by applying Karhunen-Loève (K-L) expansion (e.g., [26,15]). By collecting an ensemble of the system solution data from process historical data or simulation data, the K-L expansion method considers the presence of the dominant spatial patterns in the solution of the parabolic PDEs and results in a more comprehensive and accurate ROM than a ROM based on analytical basis functions. This data-based construction of the basis functions for order reduction to PDE systems has been widely adopted in the recent years in the context of model-based control problems for parabolic PDE systems (e.g., [4,27,2,1,28,22]).

In this work, several EMPC systems are formulated and applied to a non-isothermal tubular reactor where a second-order chemical reaction takes place. First, an output feedback EMPC formulation is presented. Second, a reduced-order model (ROM) of the PDEs is constructed on the basis of historical data-based empirical eigenfunctions by applying Karhunen-Loève expansion to use in the formulation of a computationally efficient EMPC system. Several EMPC systems each using a different ROM (i.e., different number of modes and derived from either using analytical sinusoidal/cosinusoidal eigenfunctions or empirical eigenfunctions) are applied to the non-isothermal tubular reactor example. The model accuracy, computational time and closed-loop economic performance of the closed-loop tubular reactor under the different EMPC systems are compared and discussed.

2. Preliminaries

2.1. Parabolic PDEs

We consider quasi-linear parabolic PDEs with measured outputs of the form:

$$\frac{\partial \bar{x}}{\partial t} = A\frac{\partial \bar{x}}{\partial z} + B\frac{\partial^2 \bar{x}}{\partial z^2} + Wu(t) + f(\bar{x}(z,t)) \tag{1}$$

$$y_j(t) = \int_0^1 c_j(z)\bar{x}(z,t)dz \tag{2}$$

for $j = 1, \ldots, p$, with the boundary conditions:

$$\left.\frac{\partial \bar{x}}{\partial z}\right|_{z=0} = g_0\bar{x}(0,t), \quad \left.\frac{\partial \bar{x}}{\partial z}\right|_{z=1} = g_1\bar{x}(1,t) \tag{3}$$

for $t \in [0, \infty)$ and the initial condition:

$$\bar{x}(z,0) = \bar{x}_0(z) \tag{4}$$

where $z \in [0, 1]$ is the spatial coordinate, $t \in [0, \infty)$ is the time, $\bar{x}'(z,t) = [\bar{x}_1(z,t) \cdots \bar{x}_{n_x}(z,t)]$ is the vector of the state variables ($\bar{x}'$ denotes the transpose of $\bar{x}$), $f(\bar{x}(z,t))$ denotes a nonlinear vector function, $y_j(t)$ is the j-th measured output, and $c_j(z)$ are known smooth functions of z ($j = 1, \ldots, p$) whose functional form depends on the type of the measurement sensor. The notation A, B, W, g_0 and g_1 is used to denote (constant) matrices of appropriate dimensions. The control input vector is denoted as $u(t) \in \mathbb{R}^{n_u}$ and is subject to the following constraints:

$$u_{\min} \le u(t) \le u_{\max} \tag{5}$$

where $u_{\min}$ and $u_{\max}$ are the lower and upper bound vectors of the manipulated input vector, $u(t)$. Moreover, the system states are also subject to the following state constraints:

$$x_{i,\min} \le \int_0^1 r_{x_i}(z)\bar{x}_i(z,t)dz \le x_{i,\max}, \quad i = 1, \ldots, n_x \tag{6}$$

where $x_{i,\min}$ and $x_{i,\max}$ are the lower and upper state constraint for the i-th state, respectively. The function $r_{x_i}(z) \in L_2(0,1)$ where $L_2(0,1)$ is the space of measurable, square-integrable functions on the interval $[0, 1]$ is the state constraint distribution function.

2.2. Galerkin's method

We first formulate the PDE system of Eqs. (1)–(4) as an infinite dimensional system in the Hilbert space $\mathcal{H}([0,1]; \mathbb{R}^{n_x})$, with $\mathcal{H}$ being the space of measurable vector functions defined on $[0, 1]$, with inner product and norm:

$$(\omega_1, \omega_2) = \int_0^1 (\omega_1(z), \omega_2(z))_{\mathbb{R}^{n_x}} dz, \qquad \|\omega_1\|_2 = (\omega_1, \omega_1)^{\frac{1}{2}} \tag{7}$$

where ω_1, ω_2 are two elements of $\mathcal{H}([0,1]; \mathbb{R}^{n_x})$ and the notation $(\cdot, \cdot)_{\mathbb{R}^{n_x}}$ denotes the standard inner product in $\mathbb{R}^{n_x}$. The state function $x(t)$ on the state-space $\mathcal{H}$ is defined as

$$x(t) = \bar{x}(z,t), \quad t > 0, \quad 0 \le z \le 1, \tag{8}$$

and the operator $\mathcal{A}$ is defined as

$$\mathcal{A}x = A\frac{d\bar{x}}{dz} + B\frac{d^2\bar{x}}{dz^2}, \quad 0 \le z \le 1. \tag{9}$$

and the measured output operator is defined as:

$$\mathcal{C}x(t) = \left[(c_1(\cdot), \bar{x}(\cdot, t)), \ldots, (c_p(\cdot), \bar{x}(\cdot, t))\right]' \tag{10}$$

Then, the system of Eqs. (1)–(4) takes the following form:

$$\dot{x}(t) = \mathcal{A}x(t) + \mathcal{B}u(t) + \mathcal{F}(x(t)), \quad x(0) = x_0 \tag{11}$$

$$y(t) = \mathcal{C}x(t) \tag{12}$$

where $x_0 = \bar{x}_0(z)$, $\mathcal{B}u(t) = Wu(t)$ and $\mathcal{F}(x(t))$ is a nonlinear vector function in the Hilbert space. The eigenvalue problem for $\mathcal{A}$ takes the form

$$\mathcal{A}\phi_k = \lambda_k\phi_k, \quad k = 1, \ldots, \infty \tag{13}$$

subject to

$$\left.\frac{d\phi_k}{dz}\right|_{z=0} = g_0\phi_k(0), \quad \left.\frac{d\phi_k}{dz}\right|_{z=1} = g_1\phi_k(1) \tag{14}$$

where ϕ_k is an eigenfunction corresponding to the k-th eigenvalue λ_k and $\bar{\phi}_k$ is an adjoint eigenfunction of the operator $\mathcal{A}$.

Assumption 1 below characterizes the class of parabolic PDEs considered in this work and states that the eigenspectrum of operator $\mathcal{A}$ can be partitioned into a finite part consisting of m slow eigenvalues which are close to the imaginary axis and a stable infinite complement containing the remaining fast eigenvalues which are far in the left-half of the complex plane, and that the separation between the slow and fast eigenvalues of $\mathcal{A}$ is large. We also note that the large separation of slow and fast modes of the spatial operator in parabolic PDEs ensures that a controller which exponentially stabilizes the closed-loop ODE system, also stabilizes the closed-loop infinite-dimensional system [3]. This assumption is satisfied by the majority of diffusion–convection–reaction processes [5].

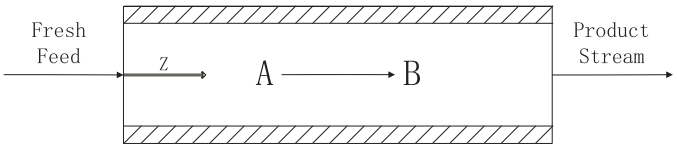

Fig. 1. A tubular reactor with reaction A → B.

Assumption 1.

1. $Re(\lambda_1) \geq Re(\lambda_2) \geq \cdots \geq Re(\lambda_k) \geq \cdots$, where $Re(\lambda_k)$ denotes the real part of the eigenvalue, λ_k.
2. The eigenspectrum of $\mathcal{A}$, $\sigma(\mathcal{A})$, is defined as the set of all eigenvalues of $\mathcal{A}$, i.e., $\sigma(\mathcal{A}) = \{\lambda_1, \lambda_2, \ldots\}$. $\sigma(\mathcal{A})$ can be partitioned as $\sigma(\mathcal{A}) = \sigma_1(\mathcal{A}) \cup \sigma_2(\mathcal{A})$, where $\sigma_1(\mathcal{A})$ consists of the first m finite eigenvalues, i.e., $\sigma_1(\mathcal{A}) = \{\lambda_1, \ldots, \lambda_m\}$, and $|Re(\lambda_1)|/|Re(\lambda_m)| = O(1)$.
3. $Re(\lambda_{m+1}) < 0$ and $|Re(\lambda_1)|/|Re(\lambda_{m+1})| = O(\epsilon)$ where $\epsilon < 1$ is a small positive number.

Next, we apply standard Galerkin's method [23] to the infinite-dimensional system of Eqs. (11) and (12) to derive a finite-dimensional subsystem. Let $\mathcal{H}_s$ and $\mathcal{H}_f$ be modal subspaces of $\mathcal{A}$ defined as $\mathcal{H}_s = \text{span}\{\phi_1, \phi_2, \ldots, \phi_m\}$ and $\mathcal{H}_f = \text{span}\{\phi_{m+1}, \phi_{m+2}, \ldots\}$, where ϕ_k, $k = 1, 2, \ldots$ are the eigenfunctions of $\mathcal{A}$. Using the orthogonal projection operators, P_s and P_f, which project the state x onto the subspaces $\mathcal{H}_s$ and $\mathcal{H}_f$ of $\mathcal{A}$, respectively ($x_s = P_s x \in \mathcal{H}_s$ and $x_f = P_f x \in \mathcal{H}_f$), the state x of the system of Eq. (11) can be written as

$$x = x_s + x_f = P_s x + P_f x \tag{15}$$

Applying P_s and P_f to the system of Eqs. (11) and (12) and using the above decomposition for x, Eqs. (11) and (12) can be re-written as:

$$\begin{aligned} \dot{x}_s(t) &= \mathcal{A}_s x_s(t) + \mathcal{F}_s(x_s(t), x_f(t)) + \mathcal{B}_s u(t), \quad x_s(0) = P_s x_0, \\ \dot{x}_f(t) &= \mathcal{A}_f x_f(t) + \mathcal{F}_f(x_s(t), x_f(t)) + \mathcal{B}_f u(t), \quad x_f(0) = P_f x_0, \\ y(t) &= \mathcal{C}_s x_s(t) + \mathcal{C}_f x_f(t) \end{aligned} \tag{16}$$

where $\mathcal{A}_s = P_s\mathcal{A}$, $\mathcal{B}_s = P_s\mathcal{B}$, $\mathcal{A}_f = P_f\mathcal{A}$, $\mathcal{B}_f = P_f\mathcal{B}$, $\mathcal{F}_f = P_f\mathcal{F}$, $\mathcal{F}_s = P_s\mathcal{F}$, $\mathcal{C}_s = \mathcal{C}P_s$, and $\mathcal{C}_f = \mathcal{C}P_f$. Specifically, $\mathcal{A}_s = \text{diag}\{\lambda_k\}$, $k = 1, \ldots, m$ is a diagonal matrix of dimension $m \times m$ and may contain unstable eigenvalues (i.e., $Re(\lambda_k) > 0$ for some k). Since the basis functions ϕ_k are the eigenfunctions of $\mathcal{A}$, the eigenfunctions ϕ_k are orthogonal to each other. Furthermore, the subspaces of $\mathcal{A}$, $\mathcal{H}_s$ and $\mathcal{H}_f$, are spanned by the eigenfunctions ϕ_k (of the operator $\mathcal{A}$), and then, $\mathcal{A}_s x_f \equiv 0$ and $\mathcal{A}_f x_s \equiv 0$. Also, the operator $\mathcal{A}_f$ is an unbounded exponentially stable differential operator. The first subsystem (i.e., first equation) of Eq. (16) is referred to as the slow subsystem; while, the second subsystem is referred to as the fast subsystem. Neglecting the fast subsystem, we obtain the ODE system describing the dominant dynamics of the PDE:

$$\begin{aligned} \dot{x}_s(t) &= \mathcal{A}_s x_s(t) + \mathcal{F}_s(x_s(t), 0) + \mathcal{B}_s u(t), \quad x_s(0) = P_s x_0 \\ y(t) &= \mathcal{C}_s x_s(t) \end{aligned} \tag{17}$$

2.3. Tubular reactor example

A chemical process example of industrial importance of the form of Eq. (1) is used to demonstrate the EMPC systems formulated in this work. Specifically, consider a tubular reactor shown in Fig. 1, where an exothermic, irreversible second-order reaction of the form A → B takes place. A cooling jacket of constant temperature is used to remove heat from the reactor. The states of the tubular reactor are temperature and concentration of A in the reactor, and the input is the inlet concentration of A. In order to simplify the presentation of our results below, we use dimensionless variables and obtain the following nonlinear parabolic PDE model for the process (details and model notation can be found in [20,23]):

$$\begin{aligned} \frac{\partial \bar{x}_1}{\partial t} &= -\frac{\partial \bar{x}_1}{\partial z} + \frac{1}{Pe_1}\frac{\partial^2 \bar{x}_1}{\partial z^2} + B_T B_C \exp\left(\frac{\gamma \bar{x}_1}{1+\bar{x}_1}\right)(1+\bar{x}_2)^2 + \beta_T(T_s - \bar{x}_1) + \delta(z-0)T_i \\ \frac{\partial \bar{x}_2}{\partial t} &= -\frac{\partial \bar{x}_2}{\partial z} + \frac{1}{Pe_2}\frac{\partial^2 \bar{x}_2}{\partial z^2} - B_C \exp\left(\frac{\gamma \bar{x}_1}{1+\bar{x}_1}\right)(1+\bar{x}_2)^2 + \delta(z-0)u \end{aligned} \tag{18}$$

where δ is the standard Dirac function, subject to the following boundary conditions:

$$\begin{aligned} z = 0 &: \frac{\partial \bar{x}_1}{\partial z} = Pe_1 \bar{x}_1, \quad \frac{\partial \bar{x}_2}{\partial z} = Pe_2 \bar{x}_2; \\ z = 1 &: \frac{\partial \bar{x}_1}{\partial z} = 0, \quad \frac{\partial \bar{x}_2}{\partial z} = 0; \end{aligned} \tag{19}$$

The following typical values are given to the process parameters: $Pe_1 = 7$, $Pe_2 = 7$, $B_T = 2.5$, $B_C = 0.1$, $\beta_T = 2$, $T_s = 0$, $T_f = 0$ and $\gamma = 10$. In all simulations reported below, second-order finite-difference method was used to discretize, in space, the two parabolic PDEs of Eq. (18) to derive two 101th-order set of ODEs (further increase on the order of discretization led to identical open-loop and closed-loop results); this discretized model was used to describe the process dynamics. The following simulations were carried out using Java programming language in a Intel Core $i7-2600$, 3.40 GHz computer with a 64-bit Windows 7 Professional operating system.

3. Methodological framework for output feedback EMPC for PDE systems

3.1. State-estimation using output feedback methodology

The objective of this section is to propose state estimation-based EMPC formulations that make use of a finite number, p, of measured outputs $y_j(t)$ ($j = 1, \ldots, p$) to compute estimates of x_s and x_f. The state estimation scheme is based on a direct inversion of the measured output operator to obtain estimates of the slow modes, $\hat{x}_s(t)$ and the concept of the approximate inertial manifolds to obtain estimates of the fast modes, $\hat{x}_f(t)$ in the system of Eq. (16). To develop this estimation scheme, we must impose an assumption on the number of measured outputs. We assume that the number of measured outputs is equal to the number of slow modes (i.e., $p = m$) and the distribution functions of the measured outputs are chosen such that $\mathcal{C}_s^{-1}$ exists. Under this assumption, an estimate of the slow subsystem state, $\hat{x}_s(t)$ can be obtained as follows:

$$\hat{x}_s(t) = \mathcal{C}_s^{-1} y(t) \tag{20}$$

where $\hat{x}_s(t)$ is an estimate of $x_s(t)$.

Since the accuracy of the estimated modes through the reconstruction of the spatially distributed PDE states is limited by the number of available measurement points, we introduce the derivation of the estimation for the fast subsystem state, $x_f(t)$ to achieve additional accuracy of the state estimation scheme. In the infinite-dimensional system described by Eq. (16), the fast dynamics, $\dot{x}_f(t)$ can be ignored compared with that of the slow dynamics, $\dot{x}_s(t)$ given that $\mathcal{A}_f$ includes eigenvalues with large negative real part [5] ($\mathcal{A}_f$ is exponentially stable). Thus, the equation of the fast state, $x_f(t)$ can be approximately expressed as the following equality:

$$\mathcal{A}_f x_f(t) + \mathcal{B}_f u(t) + \mathcal{F}_f(x_s(t), x_f(t)) = 0 \tag{21}$$

The fast state x_f is equal to zero at its quasi-steady-state (we note that $\bar{x}(z,t)=0$ is a steady-state of the nominal PDE system $u(t)\equiv 0$). Accounting for the fact that $\mathcal{A}_f$ includes eigenvalues with large negative real parts, we can neglect the fast subsystem state, $x_f(t)$ in the nonlinear term, $\mathcal{F}_f(x_s, x_f)$. Using the estimated slow subsystem state, $\hat{x}_s$ to calculate the approximate fast subsystem state, Eq. (21) becomes

$$\mathcal{A}_f\hat{x}_f(t)+\mathcal{B}_f u(t)+\mathcal{F}_f(\hat{x}_s(t),0)=0 \tag{22}$$

where $\hat{x}_f(t)$ is the estimated fast state. An explicit form for the estimated fast state can be derived:

$$\hat{x}_f(t)=-\mathcal{A}_f^{-1}[\mathcal{B}_f u(t)+\mathcal{F}_f(\hat{x}_s(t),0)] \tag{23}$$

Remark 1. The accuracy of the finite-dimensional ODE model with m slow modes is of order $\epsilon=|Re\{\lambda_1(\mathcal{A})\}|/|Re\{\lambda_{m+1}(\mathcal{A})\}|$ ($O(\epsilon)$). This means under state feedback the closeness of the closed-loop system PDE state to the closed-loop system ODE state is $O(\epsilon)$. Closed-loop stability under output feedback works not only for the slow and fast modes but also the real state as long as the estimation error is negligible. This occurs when m is chosen to be sufficiently large such that ϵ is sufficiently small. Specifically, to achieve the same level of closeness for the output feedback case ($O(\epsilon)$), the number of measurements must be equal to the number of slow modes (i.e., $p=m$). From a practical standpoint, the discrepancy between the closed-loop PDE state under output feedback with more than m measurements and the one of the closed-loop PDE state under output feedback with m measurements will be indistinguishable since the achieved closed-loop system performance is limited by the number of slow modes (m) used in the design of the EMPC. Therefore, if there are more available measurement points than the slow modes ($p>m$), one can pick any m measurement points from the set of p points as long as the assumption that $\mathcal{C}_s^{-1}$ exists is satisfied. In this work, from both the open-loop and closed-loop system simulation, we have good state estimation accuracy by picking m sufficiently large and choosing the measurement points such that the inverse of the matrix $\mathcal{C}_s$ exists.

3.2. Output feedback economic model predictive control formulation

Utilizing the estimates $\hat{x}_s$ and $\hat{x}_f$ of Eqs. (20) and (23), respectively, we formulate a state estimation-based Lyapunov-based EMPC for the system of Eq. (16) to dynamically optimize an economic cost function. We assume that the output measurements are available continuously and synchronously at sampling instants denoted as $t_k=k\Delta$ with $k=0,1,\ldots$. Accounting for x_f is important for increasing PDE state estimation accuracy and satisfying state constraints. To formulate a finite-dimensional EMPC problem, the fast subsystem is truncated at the l-th fast state. With the estimated slow and fast modes, of Eqs. (20) and (23), respectively, the EMPC formulation takes the following form:

$$\max_{u\in S(\Delta)} \int_{t_k}^{t_{k+N}} L(\check{x}(\tau),u(\tau))d\tau \tag{24a}$$

$$\text{s.t.}\quad \dot{\tilde{x}}_s(t)=\mathcal{A}_s\tilde{x}_s(t)+\mathcal{F}_s(\tilde{x}_s(t),\tilde{x}_f(t))+\mathcal{B}_s u(t) \tag{24b}$$

$$\tilde{x}_s(t_k)=\mathcal{C}_s^{-1}y(t_k) \tag{24c}$$

$$\tilde{x}_f(t)=-\mathcal{A}_f^{-1}[\mathcal{B}_f u(t)+f_f(\tilde{x}_s(t),0)] \tag{24d}$$

$$\check{x}(t)=\tilde{x}_s(t)+\tilde{x}_f(t) \tag{24e}$$

$$u_{\min}\le u(t)\le u_{\max},\quad \forall t\in[t_k,t_{k+N}) \tag{24f}$$

$$x_{i,\min}\le(r_{x_i},\check{x}_i(t))\le x_{i,\max},\quad i=1,\ldots,n_x,\quad \forall t\in[t_k,t_{k+N}) \tag{24g}$$

$$\check{x}\prime(t)P\check{x}(t)\le\overline{\rho} \tag{24h}$$

where Δ is the sampling period, $S(\Delta)$ is the family of piecewise constant functions with sampling period Δ, N is the prediction horizon, $\tilde{x}_s(t)$ and $\tilde{x}_f(t)$ are the predicted evolution of the slow subsystem state and fast subsystem state, respectively, with input $u(t)$ computed by the EMPC and $y(t_k)$ is the output measurement at the sampling time t_k.

In the optimization problem of Eq. (24), the objective function of Eq. (24a) describes the dynamic economics of the process which the EMPC maximizes over a horizon t_N. The constraint of Eq. (24b) is used to predict the future evolution of the slow subsystem with the initial condition given in Eq. (24c) (i.e., the estimate of $x_s(t_k)$ computed from the output $y(t_k)$). The constraint of Eq. (24d) is the finite-dimensional truncation of the fast subsystem which is used to predict the evolution of the fast subsystem states. The symbol $\check{x}(t)$ is used to denote the finite dimensional truncated state vector (i.e., both the slow subsystem and the fast subsystem states). The constraints of Eqs. (24f)–(24g) are the available control action and the state constraints, respectively. Finally, the constraint of Eq. (24h) ensures that the predicted state trajectory is restricted inside a predefined stability region which is a level set of the Lyapunov function (see [13] for a complete discussion of this issue). The optimal solution to this optimization problem is $u^*(t|t_k)$ defined for $t\in[t_k,t_{k+N})$. The EMPC applies the control action computed for the first sampling period to the system in a sample-and-hold fashion for $t\in[t_k,t_{k+1})$. The EMPC is resolved at the next sampling period, t_{k+1}, after receiving a new output measurement, $y(t_{k+1})$.

Remark 2. In the formulation of the state estimation-based Lyapunov-based EMPC of Eq. (24), Eq. (24h) defines a stability region of the closed-loop system. This stability region is typically characterized with an explicit stabilizing state feedback controller [13,14]. To account for the fact that additional uncertainty may be introduced by using an output feedback controller over a state feedback controller due to the estimation error, the stability region, computed using an explicit stabilizing state feedback controller, may be reduced for the output feedback case and a sufficiently large number of slow modes m (as well as number of output measurements p) can always be found to ensure that closed-loop stability under output feedback is accomplished.

3.3. Implementation of output feedback EMPC

The output feedback EMPC is applied to the tubular reactor. To solve the EMPC problem, the open-source interior point solver Ipopt [29] was used. Explicit Euler's method was used with sufficiently small integration step of 1×10^{-4} to numerically integrate the finite-dimensional ODE model of the transport-reaction process. The cost function that we consider is to maximize the overall reaction rate along the length of the reactor. The economic cost that the EMPC works to maximize over the prediction horizon is

$$L(\bar{x},u)=\int_0^1 r(z,t)dz \tag{25}$$

where

$$r(z,t)=B_C\exp\left(\frac{\gamma\bar{x}_1}{1+\bar{x}_1}\right)(1+\bar{x}_2)^2 \tag{26}$$

is the reaction rate.

Regarding input and state constraints, the manipulated input is subject to constraints as follows: $-1\le u\le 1$. Owing to economic considerations, the amount of reactant material available over the period t_f is fixed. Specifically, the input trajectory should satisfy:

$$\frac{1}{t_f}\int_0^{t_f}u(\tau)\,d\tau=0.5 \tag{27}$$

where $t_f = 1.0$. To simplify the notation, we use the notation $u \in g(t_k)$ to denote this constraint. Constraints on the minimum and maximum temperatures along the length of the reactor are considered as state constraints, Namely, the temperature along the length of the reactor must satisfy the following inequalities:

$$x_{1,\min} \le \bar{x}_1(z,t) \le x_{1,\max} \tag{28}$$

for all $z \in [0, 1]$ where $x_{1,min} = -1$ and $x_{1,max} = 3$ are the lower and upper limits, respectively.

Since the PDE system of Eq. (18) consists of two PDEs, the index i ($i = 1, 2$) is used to denote the i-th PDE of Eq. (18). We assume the tubular reactor has $p_1 + p_2$ sensors where the first p_1 sensors measure the temperature (i.e., the state corresponding to the first PDE of Eq. (18)) at measurement points $z_{s,1j} \in [0, 1]$ for $j = 1, 2, \ldots, p_1$, and the next p_2 sensors measure the concentration of A (i.e., the second state) at measurement points $z_{s,2j} \in [0, 1]$ for $j = 1, 2, \ldots, p_2$. Thus, the output measurements consist of the state measurements at a finite number of points in the spatial domain (i.e., $x_i'(t_k) = [x_i(z_{s,i1}, t_k) \cdots x_i(z_{s,ip_i}, t_k)]$) and can be written as

$$y_{ij}(t_k) = \bar{x}_i(z_{s,ij}, t_k), \quad i = 1, 2, \quad j = 1, 2, \ldots, p_i$$

where the output measurement vector, $y'(t_k) = [y_1'(t_k) y_2'(t_k)]$ and

$$y_i'(t_k) = [y_{i1}(t_k) \cdots y_{ip_i}(t_k)], \quad i = 1, 2.$$

We assume the number of measurements satisfies $p_i = m_i$ where m_i refers to the number of total slow modes retained from the i-th PDE in the construction of the model of Eq. (24b). Since pointwise measurements are considered, the following measurement distribution function is used:

$$c_{ij}(z) = \delta(z - z_{s,ij}), \quad i = 1, 2, \quad j = 1, 2, \ldots, p_i \tag{29}$$

where δ is the standard Dirac function. Each measurement point, $z_{s,ij}$ in the spatial domain is assumed to be at $z_{s,ij} = (j-1)/(p_i - 1)$. The choice of measurement points satisfies the assumption that $\mathcal{C}_{s,i}^{-1}$ exists.

The state $\bar{x}_i(z,t)$ can be decomposed into the sum of the amplitudes and the eigenfunctions of the first l_i eigenmodes:

$$\bar{x}_i(z,t) \approx \sum_{j=1}^{l_i} a_{ij}(t)\phi_{ij}(z), \quad i = 1, 2 \tag{30}$$

where $a_{ij}(t)$ and $\phi_{ij}(z)$ are the amplitude and eigenfunctions associated with the j-th eigenvalue of the spatial operator $\mathcal{A}$. Utilizing the decomposition of Eq. (30), the estimated slow mode vector, $a_{s,i}'(t_k) = [a_{s,i1}(t_k) \cdots a_{s,ip_i}(t_k)]$ (recall that $m_i = p_i$) can be written in the following form:

$$y_i(t_k) = \mathcal{C}_{s,i} x_i(t_k) = C_{s,i} a_{s,i}(t_k) = \begin{pmatrix} \phi_{i1}(z_{s,i1}) & \phi_{i2}(z_{s,i1}) & \cdots & \phi_{ip}(z_{s,i1}) \\ \phi_{i1}(z_{s,i2}) & \phi_{i2}(z_{s,i2}) & \cdots & \phi_{ip}(z_{s,i2}) \\ \vdots & \vdots & \ddots & \vdots \\ \phi_{i1}(z_{s,ip_i}) & \phi_{i2}(z_{s,ip_i}) & \cdots & \phi_{ip}(z_{s,ip_i}) \end{pmatrix} \begin{pmatrix} a_{s,i1}(t_k) \\ a_{s,i2}(t_k) \\ \vdots \\ a_{s,ip_i}(t_k) \end{pmatrix} \tag{31}$$

for $i = 1, 2$. The estimated slow modes are:

$$\hat{a}_{s,i}(t_k) = C_{s,i}^{-1} y_i(t_k) = \begin{pmatrix} \phi_{i1}(z_{s,i1}) & \phi_{i2}(z_{s,i1}) & \cdots & \phi_{ip}(z_{s,i1}) \\ \phi_{i1}(z_{s,i2}) & \phi_{i2}(z_{s,i2}) & \cdots & \phi_{ip}(z_{s,i2}) \\ \vdots & \vdots & \ddots & \vdots \\ \phi_{i1}(z_{s,ip_i}) & \phi_{i2}(z_{s,ip_i}) & \cdots & \phi_{ip}(z_{s,ip_i}) \end{pmatrix}^{-1} \begin{pmatrix} \bar{x}_i(z_{s,i1}, t_k) \\ \bar{x}_i(z_{s,i2}, t_k) \\ \vdots \\ \bar{x}_i(z_{s,ip_i}, t_k) \end{pmatrix} \tag{32}$$

where $\hat{a}_{s,i}(t_k)$ is an estimate of $a_{s,i}(t_k)$ from the output measurement, $y(t_k)$.

Since the decomposition of Eq. (30) provides a simplified method for describing the temporal evolution of the PDE system, the reduced-order model used in the EMPC (Eqs. (24b) and (24d)) is written in terms of the temporal evolution of the amplitudes of each eigenmode. After applying the decomposition of Eq. (30) to Eq. (16), multiplying both sides by the adjoint eigenfunction, and making a similar approximation as in Eq. (23), the resulting reduced-order model has the following form (the $\hat{}$ notation is dropped for simplicity of presentation):

$$\begin{aligned} \dot{a}_{s,i}(t) &= A_{s,i} a_{s,i}(t) + F_{s,i}(a_s(t), a_f(t)) + B_{s,i} u(t), \\ a_{f,i}(t) &= A_{f,i}^{-1} \left[B_{f,i} u(t) + F_{f,i}(a_s(t), a_f(t)) \right], \quad i = 1, 2 \\ y(t) &= C_{s,1} a_{s,1}(t) + C_{s,2} a_{s,2}(t) + C_{f,1} a_{f,1}(t) + C_{f,2} a_{f,2}(t) \end{aligned} \tag{33}$$

where $a_{s,i}(t) = [a_{s,i1}(t) \;\; a_{s,i2}(t) \cdots a_{s,im_i}(t)]'$ with elements $a_{s,ij}(t) \in \mathbb{R}$ associated with the amplitudes of the j-th eigenmodes. The vector $a_{f,i}(t)$ is a vector of similar structure to $a_{s,i}(t)$ with elements associated with the next $m_i + 1$ to l_i eigenmodes. The vector $a_s(t)$ and $a_f(t)$ are defined as $a_s(t) = [a_{s,1}(t) a_{s,2}(t)]'$ and $a_f(t) = [a_{f,1}(t) a_{f,2}(t)]'$. Using this notation, the matrix $A_{s,i}$ is defined as $A_{s,i} = \mathrm{diag}\{\lambda_{ij}\}, j = 1, \ldots, m_i$ (i.e., a diagonal $m_i \times m_i$ matrix where diagonal entries are equal to λ_{ij} and the indices j and i are used to denote the j-th eigenmode of the i-th PDE state) and the matrix $A_{f,i}$ is defined as $A_{f,i} = \mathrm{diag}\{\lambda_{ij}\}$, $j = m_i + 1, \ldots, l_i$. Therefore, the quadratic Lyapunov function of Eq. (24h) is also written in terms of the amplitudes and has the form:

$$V(a(t)) = a'(t) P a(t) \tag{34}$$

where $a(t)$ denotes a vector consisting of the amplitudes of all retained eigenmodes (i.e., both $a_s(t)$ and $a_f(t)$) for each PDE, P is an $(l_1 + l_2) \times (l_1 + l_2)$ identity matrix and $\overline{\rho} = 3$ is used in the formulations of the EMPC systems below.

3.3.1. Case 1: low-order output feedback EMPC system

In this set of simulations, a low-order output feedback EMPC system of the form of Eq. (24) (the fast modes are neglected) is formulated for the tubular reactor with the economic cost function of Eq. (25), the input constraint of Eq. (27) and the state constraint of Eq. (28). The low-order output feedback EMPC is given by the following optimization problem:

$$\max_{u \in S(\Delta)} \quad \frac{1}{N\Delta} \int_{t_k}^{t_{k+N}} \left(\int_0^1 r(z,\tau) dz \right) d\tau \tag{35a}$$

$$\text{s.t.} \quad \dot{\tilde{a}}_{s,i}(t) = A_{s,i} \tilde{a}_{s,i}(t) + F_{s,i}(\tilde{a}_s(t), 0) + B_{s,i} u(t), \quad i = 1, 2 \tag{35b}$$

$$\tilde{a}_{s,i}(t_k) = C_s^{-1} y_i(t_k), \quad i = 1, 2 \tag{35c}$$

$$-1 \le u(t) \le 1, \quad \forall t \in [t_k, t_{k+N}) \tag{35d}$$

$$u(t) \in g(t_k) \tag{35e}$$

$$-1 \le \sum_{j=1}^{m_1} \tilde{a}_{s,1j}(t)\phi_{1j}(z) \le 3 \tag{35f}$$

$$\tilde{a}_s'(t)P\tilde{a}_s(t) \le \overline{\rho} \tag{35g}$$

where the notation $\tilde{a}_s$ denotes the predicted temporal evolution of the amplitudes of the slow modes, the prediction horizon is $N=3$ and the sampling time is $\Delta=0.01$. The constraint of Eq. (35e) is the integral input constraint of Eq. (27) formulated for the sampling time t_k on the basis of the material usage from $t=0$ to $t=t_k$ to ensure that the integral input constraint is satisfied over the window $t_f=1.0$ (for simplicity of presentation, the beginning of the operating window is denoted as $t=0$). The tubular reactor is initialized with a transient state profile (i.e., not the steady-state profile corresponding to the steady-state input $u_s=0.5$). For the reactor, two EMPC systems are formulated with the following low-order model of the PDE system:

1. The low-order model based on 11 slow modes only (i.e., $m_1=m_2=11$).
2. The low-order model based on 21 slow modes only (i.e., $m_1=m_2=21$).

where the measured output points consists of the state measurements at $m_1=11$ or $m_1=21$ points which are evenly spaced in the spatial domain. Additionally, the reactor under uniform in time distribution of the reactant material over $t_f=1.0$ is also considered for comparison purposes.

The closed-loop state profiles of the reactor over one period $t_f=1.0$ under the output feedback EMPC formulated with the low-order model based on 21 slow modes is displayed in Figs. 2 and 3. The computed manipulated input profiles from the low-order output feedback EMPC systems formulated based on 11 and 21 slow modes, respectively, over one period are shown in Fig. 4. From Fig. 4, the output feedback EMPC system based on 21 slow modes computes a smoother manipulated input profile than that of the output feedback EMPC system based on 11 slow modes. The maximum temperature profiles of the tubular reactor under the EMPC systems are shown in Fig. 5. Since the temperature directly influences the reaction rate, the optimal operating strategy is to operate the reactor at the maximum allowable temperature. From Fig. 5, both EMPC systems operate the tubular reactor with a maximum temperature less than the maximum allowable which is a consequence of the error associated with the low-order models. Since the low-order model based on 21 slow modes is able to more accurately compute the state profile, the output feedback EMPC system formulated with this low-order model operates the reactor at a greater temperature than the other EMPC system.

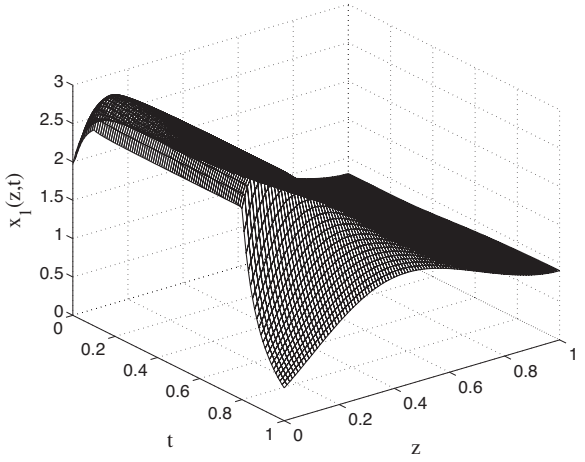

Fig. 2. Closed-loop profile of x_1 of the tubular reactor under the low-order output feedback EMPC system of Eq. (35) based on 21 slow modes over one operation period.

Over one period $t_f=1$, the total reaction rate of the process under the EMPC system based on 21 slow modes is 5.13% greater than that of EMPC system based on 11 slow modes and 8.45% greater than that of the system under uniform in time distribution of the reactant material. Moreover, the computational time profiles for these two EMPC systems of Eq. (35) is given in Fig. 6. The EMPC system based on 11 slow modes has a significant advantage in the computational efficiency since it uses fewer modes in the reduced-order model.

Remark 3. Regarding the chattering in the computed input profile (Fig. 4), the chattering is not caused by the numerical integration.

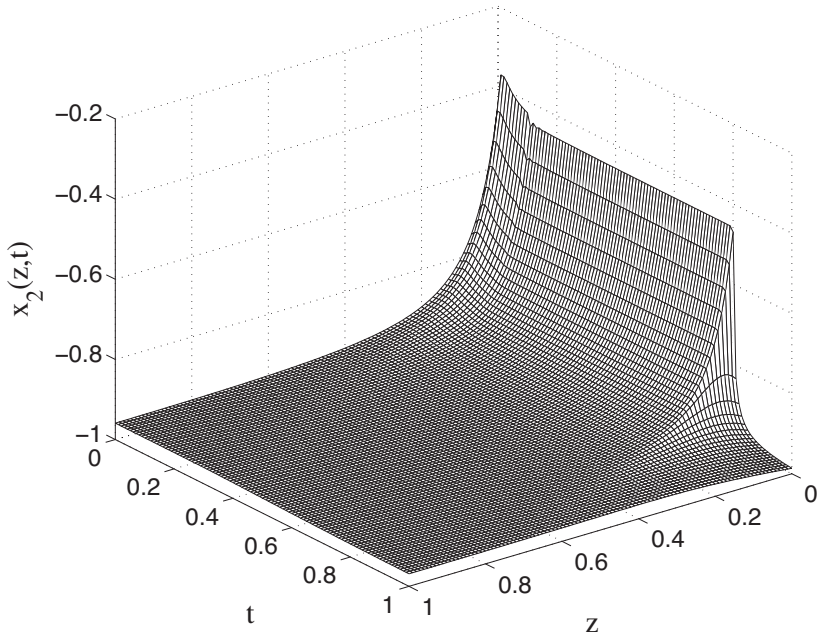

Fig. 3. Closed-loop profile of x_2 of the tubular reactor under the low-order output feedback EMPC system of Eq. (35) based on 21 slow modes over one operation period.

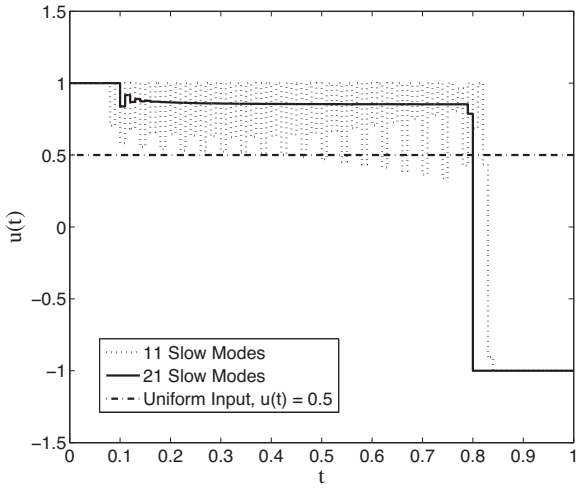

Fig. 4. Manipulated input profiles of the low-order output feedback EMPC systems of Eq. (35) based on 11 and 21 slow modes, respectively, and uniform in time distribution of the reactant material over one operation period.

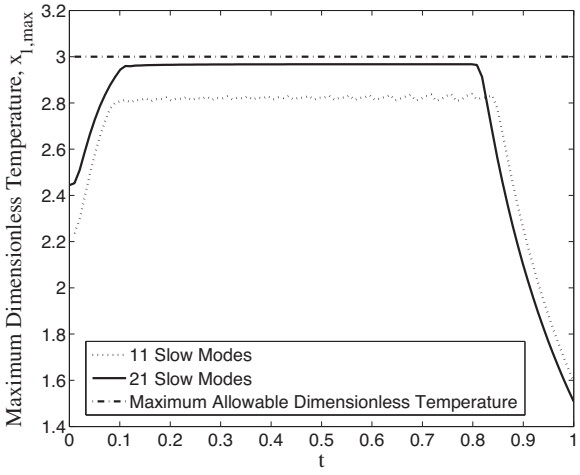

Fig. 5. Maximum temperature of x_1 profiles of the tubular reactor under the low-order output feedback EMPC systems of Eq. (35) based on 11 and 21 slow modes, respectively, over one operation period.

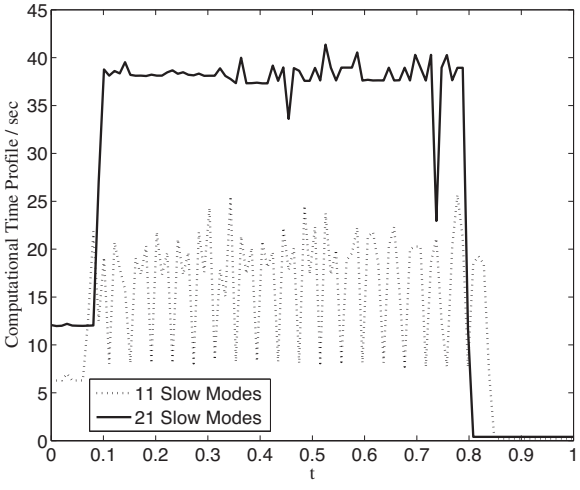

Fig. 6. Computational time profiles of the low-order output feedback EMPC system of Eq. (35) based on 11 and 21 slow modes, respectively, over one operation period.

A smaller integration time step size was tested and the same input profile was obtained.

3.3.2. Case 2: high-order output feedback EMPC system

In the second set of simulations, a high-order output feedback EMPC system of the form of Eq. (24) is formulated for the tubular reactor and has the form:

$$\max_{u\in S(\Delta)} \quad \frac{1}{N\Delta}\int_{t_k}^{t_{k+N}}\left(\int_0^1 r(z,\tau)dz\right)d\tau \tag{36a}$$

$$\text{s.t.} \quad \dot{\tilde{a}}_{s,i}(t) = A_{s,i}\tilde{a}_{s,i}(t) + F_{s,i}(\tilde{a}_s(t), \tilde{a}_f(t)) + B_{s,i}u(t) \tag{36b}$$

$$\tilde{a}_{f,i}(t) = -A_{f,i}^{-1}[B_{f,i}u(t) + F_{f,i}(\tilde{a}_s(t), 0)] \tag{36c}$$

$$\tilde{a}_{s,i}(t_k) = C_{s,i}^{-1}y_i(t_k), \quad i = 1, 2 \tag{36d}$$

$$-1 \le \sum_{j=1_1}^{l}\tilde{a}_{1j}(t)\phi_{1j}(z) \le 3 \tag{36e}$$

$$-1 \le u(t) \le 1, \quad \forall t \in [t_k, t_{k+N}) \tag{36f}$$

$$u(t) \in g(t_k) \tag{36g}$$

$$\tilde{a}'(t)P\tilde{a}(t) \le \overline{\rho} \tag{36h}$$

where $\tilde{a}_s$ is the predicted temporal evolution of the amplitudes of the slow modes, $\tilde{a}_f$ is the predicted temporal evolution of the amplitudes of the fast modes, and $\tilde{a}$ is a vector consisting of both $\tilde{a}_s$ and $\tilde{a}_f$. The prediction horizon of the EMPC is $N = 3$ and the sampling time is $\Delta = 0.01$. The high-order model of Eqs. (36b) and (36c) is based on 11 slow modes and 19 fast modes (i.e., $m_1 = m_2 = 11$ and $l_1 = l_2 = 30$). Two other model formulations are considered for comparison purposes:

1. The low-order output feedback EMPC system of Eq. (35) based on 11 slow modes.
2. A high-order EMPC system with full state feedback like in [20] based on 30 modes (11 slow modes).

Again, the system with uniform in time distribution of the reactant material over one operation period is also considered.

The closed-loop state profiles of the reactor under the high-order output feedback EMPC of Eq. (36) is displayed in Figs. 7 and 8. The manipulated input profiles computed by the high-order output feedback EMPC system of Eq. (36) is shown in Fig. 9; while, the input profile computed by the high-order state feedback EMPC system is shown in Fig. 10. From Fig. 9, chattering in the input profiles computed by the high-order output feedback EMPC systems is observed. The additional 19 fast modes in the high-order output feedback EMPC system helps reduce this compared to the low-order output feedback EMPC of Eq. (35). Correspondingly, the differences in the maximum temperature profiles among the three EMPC systems is shown in Fig. 11. The total reaction rate over one operation period of the process under the high-order output feedback EMPC system is 0.89% greater than that of the process under the low-order output feedback EMPC system and only 0.73% less than that of the process under the EMPC system with full state feedback. In summary, the above comparison results demonstrate that the additional fast modes in Eq. (36) can improve the accuracy of model prediction.

Moreover, the computational time profiles for these 3 different EMPC systems of Eq. (36) are given in Fig. 12. From Fig. 12, the computational efficiency of the EMPC system of Eq. (36) based on 30 modes (11 slow modes) is comparable to that of the full state feedback EMPC system based on 30 modes (11 slow modes). Based

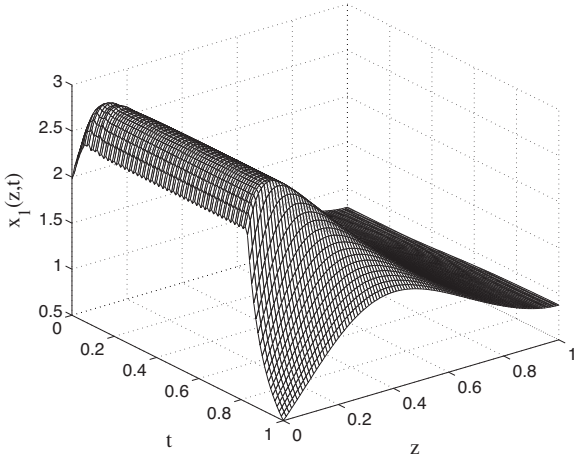

Fig. 7. Closed-loop profile of x_1 of the process under the high-order output feedback EMPC system of Eq. (36) based on 30 modes (11 slow modes) over one operation period.

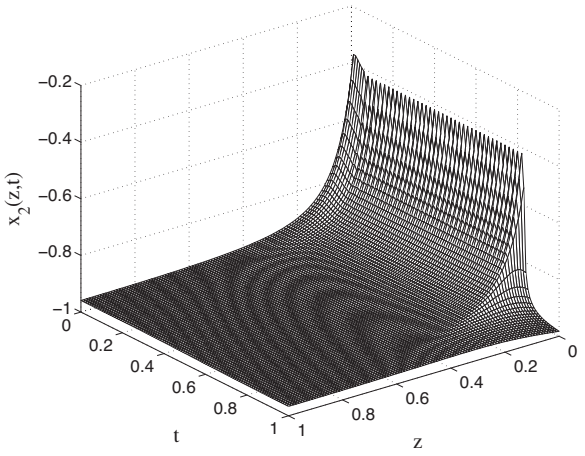

Fig. 8. Closed-loop profile of x_2 of the process under the high-order output feedback EMPC system of Eq. (36) based on 30 modes (11 slow modes) over one operation period.

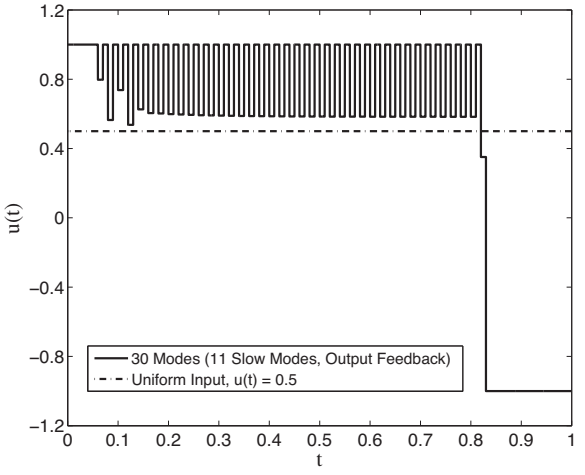

Fig. 9. Manipulated input profiles of the high-order output feedback EMPC system of Eq. (36) based on 30 modes (11 slow modes) and uniform in time distribution of the reactant material over one operation period.

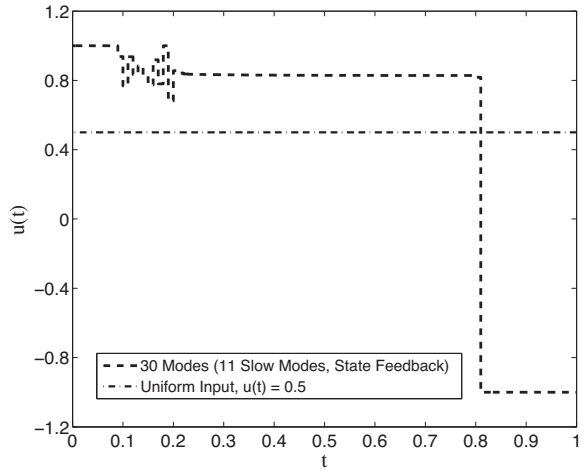

Fig. 10. Manipulated input profiles of the high-order full state feedback EMPC system based on 30 modes (11 slow modes) and uniform in time distribution of the reactant material over one operation period.

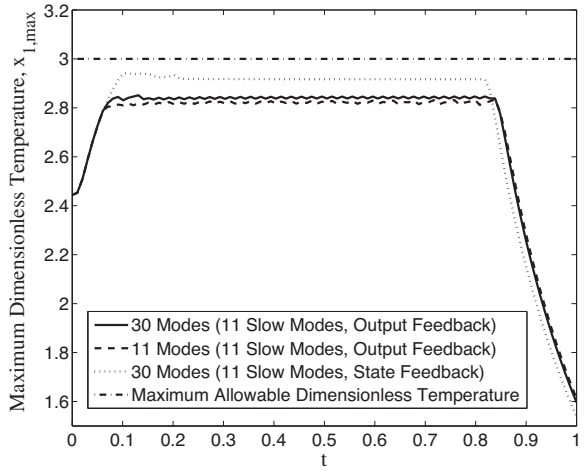

Fig. 11. Maximum temperature of x_1, profiles of the low-order output feedback EMPC system of Eq. (35) based on 11 slow modes, the high-order output feedback EMPC system of Eq. (36) based on 30 modes (11 slow modes), the high-order full state feedback EMPC system based on 30 modes (11 slow modes) over one operation period.

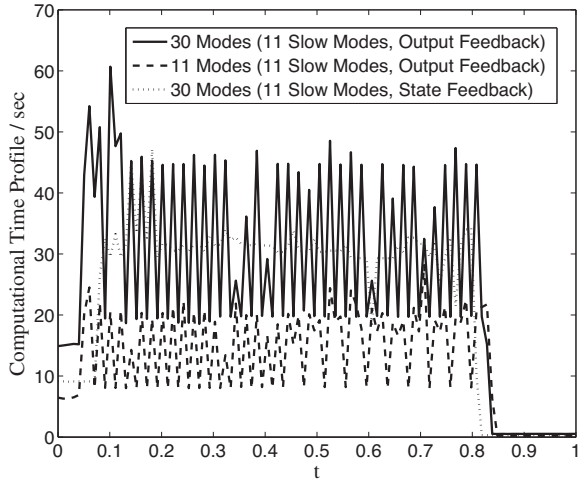

Fig. 12. Computational time profiles of the low-order output feedback EMPC system of Eq. (35) based on 11 slow modes, the high-order output feedback EMPC system of Eq. (36) based on 30 modes (11 slow modes), the high-order full state feedback EMPC system based on 30 modes (11 slow modes) over one operation period.

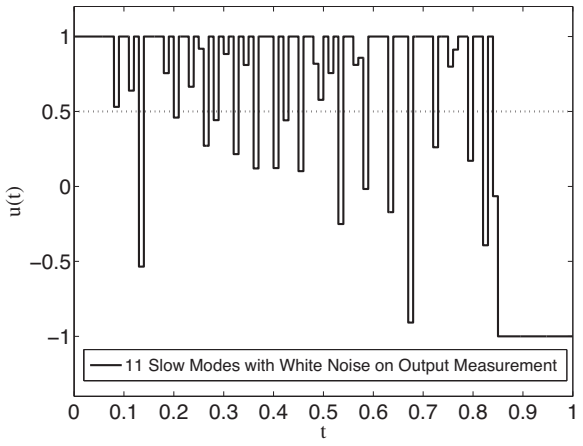

Fig. 13. Manipulated input profiles of the low-order output feedback EMPC system with white noise on output measurements (solid line). The dotted line represents uniform in time distribution of the reactant material over one operation period.

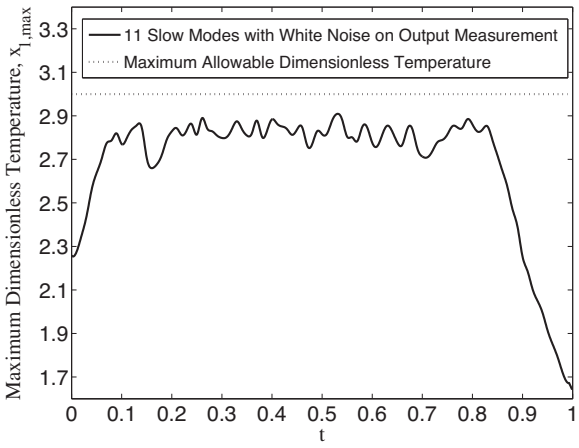

Fig. 14. Maximum temperature of x_1 profile of the low-order output feedback EMPC system with white noise on output measurement and maximum allowable dimensionless temperature over one operation period.

on the above results, from a practical point of view, comparable total economic cost and computational time is achieved while using much fewer measurement points with the high-order output feedback EMPC system than that resulting from the full state feedback EMPC system.

3.3.3. Case 3: measurement noise effect on low-order output feedback EMPC system

In this case, the effect of bounded measurement noise on the output measurements is considered. Process noise is added to each of the output measurements (recall that the output measurements consist of point-wise measurements of each of the states along the spatial domain). The process noise is modeled as bounded Gaussian white noise with 0 mean, unit variance, and bounds given by $-w_{\max,i} \leq w_i \leq w_{\max,i}$ for $i = 1, 2$ where w_i is the noise value and $w_{\max,i}$ is the bound on the noise. The bounds are given by $w_{\max,1} = 0.1$ and $w_{\max,2} = 0.1$ which corresponds to 3% and 5% of the maximum state value, respectively. The low-order output feedback EMPC system based on 11 slow modes as in Case 1 is applied to the tubular reactor. The closed-loop manipulated input profile of the reactor under the low-order output feedback EMPC is displayed in Fig. 13. Comparing Fig. 13 with the manipulated input profile of the low-order output feedback EMPC without output measurement noise in Fig. 4, the white noise causes increased chattering in the computed input profile, but the EMPC still maintains closed-loop stability (i.e., boundedness of the closed-loop state profile in a compact set). The maximum temperature profile of the closed-loop system with measurement noise under the EMPC system is shown in Fig. 14. The EMPC system can still maintain operation below the maximum allowable temperature. Furthermore, the closed-loop economic performance index (i.e., the integral of Eq. (25) with respect to time integrated over the operating window) is 4.37 for the case without measurement noise and 4.32 for the case with measurement noise (1.1% decrease in economic performance when measurement noise is added).

4. Methodological framework for low-order EMPC using empirical eigenfunctions

As another way to derive a reduced-order model (ROM) for the system of Eq. (11), empirical eigenfunctions may be used as basis functions in Galerkin's method. This method can lead to improved computational efficiency over using analytical sinusoidal/cosinusoidal eigenfunctions. In this section, the overall approach is summarized followed by several closed-loop simulations of the closed-loop tubular reactor under an EMPC with a model constructed from empirical eigenfunctions. Both state feedback and output feedback implementation of the EMPC systems formulated for the tubular reactor example are considered.

4.1. Implementation of Karhunen-Loève expansion

In order to compute the empirical eigenfunctions, we first derive and solve a high-order and convergent discretization of the PDE of Eq. (18). In detail, 20 different initial conditions and arbitrary (constant) input values, $u(t)$ were applied to the process model to get the spatiotemporal solution profiles. Consequently, from each simulation solution profile, 125 uniformly sampled solutions (which are typically called "snapshots") were taken and combined to generate an ensemble of 2500 solutions. The Karhunen-Loève (K-L) expansion was applied to the developed ensemble of solutions to compute empirical eigenfunctions that describe the dominant spatial solution patterns embedded in the ensemble where the Jacobian in the K-L expansion is calculated through a finite-difference method. After truncating the eigenfunctions with relatively small eigenvalues (smaller than 1×10^{-5}), we were left with the first 4 eigenvalues which occupy more than 99.99% of the total energy included in the entire ensemble. The first 4 of these empirical eigenfunction profiles for each state are presented in Figs. 15 and 16. Note that in contrast to the sinusoidal/cosinusoidal eigenfunctions, these empirical eigenfunctions are not symmetric with respect to the center of the spatial domain owing to the nonlinear term f and the input $u(t)$.

The methodology used to carry out the order reduction and EMPC design is summarized below.

1. Initially, we form an ensemble of solutions of the PDE system of Eq. (1) for different values of manipulated input variables $u(t)$.
2. Then, we apply Karhunen-Loève (K-L) expansion to this ensemble to derive a set of empirical eigenfunctions (dominant spatial patterns that minimize the mean square error over all the ensemble elements) [1].
3. The empirical eigenfunctions are used as basis functions within a Galerkin's model reduction framework to transform the infinite dimensional nonlinear PDE system into a ROM in the form of a low-dimensional nonlinear ODE system.
4. Finally, an EMPC formulation is developed with the ROM and applied to the tubular reactor example.

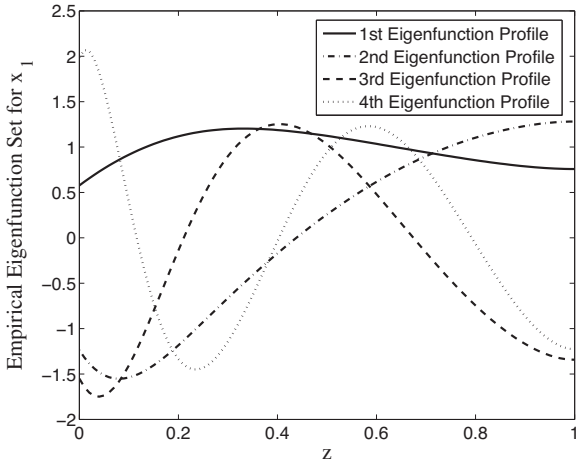

Fig. 15. First 4 empirical eigenfunction set for x_1 from an ensemble of 2500 system solutions.

Remark 4. As a practical implementation note, we point out that even though the increase of the eigenfunctions applied to the series expansion of Eq. (18) could improve the accuracy of the computed approximate model, eigenfunctions that have high frequency spatial profiles with small eigenvalues are discarded because of the probable round off errors. For this case, the descending first 5 empirical eigenvalues are listed as follows: for $\bar{x}_1(z,t)$, $\lambda_{1,1}=2.365$, $\lambda_{1,2}=1.157\times10^{-1}$, $\lambda_{1,3}=4.926\times10^{-2}$, $\lambda_{1,4}=9.315\times10^{-4}$, $\lambda_{1,5}=7.255\times10^{-6}$ and for $\bar{x}_2(z,t)$, $\lambda_{2,1}=9.719\times10^{-1}$, $\lambda_{2,2}=1.371\times10^{-1}$, $\lambda_{2,3}=5.138\times10^{-2}$, $\lambda_{2,4}=9.405\times10^{-4}$, $\lambda_{2,5}=8.930\times10^{-6}$.

4.2. Galerkin's method with empirical eigenfunctions

To reduce the PDE model of Eq. (18) into an ODE model, we take advantage of the orthogonality of the empirical eigenfunctions obtained from the K-L expansion. Specifically, using Galerkin's method, we first derive a low-order ODE system for each of the PDEs describing the temporal evolution of the amplitudes corresponding to the first m_i eigenfunctions. The low-order finite-dimensional model for the first $j=1,\ldots,m_i$ eigenfunctions of the i-th PDE has the following form:

$$\dot{a}_{s,i}(t) = A_{s,i}a_{s,i}(t) + F_{s,i}(a_s(t),0) + B_{s,i}u(t), \quad i=1,2 \tag{37}$$

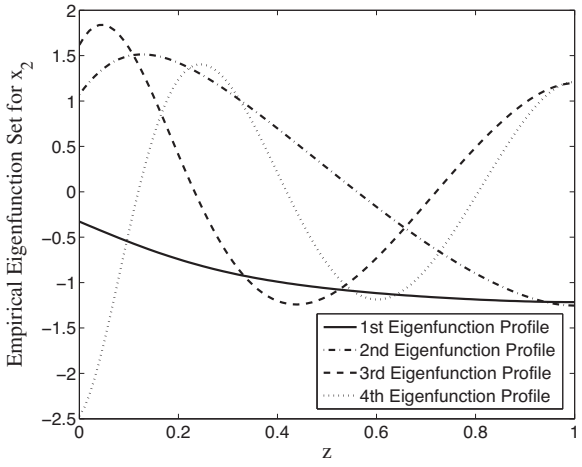

Fig. 16. First 4 empirical eigenfunction set for x_2 from an ensemble of 2500 system solutions.

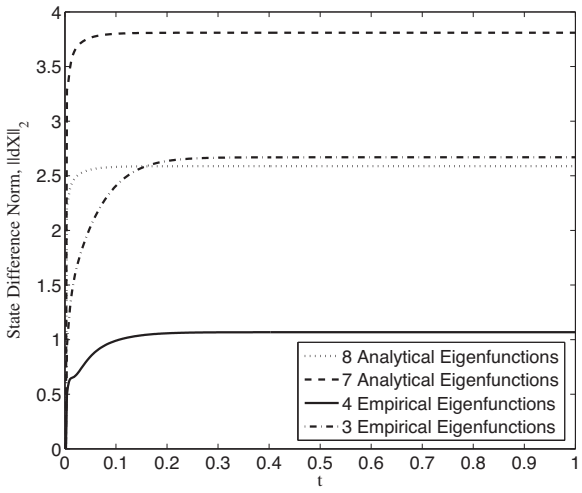

Fig. 17. L_2 norm of the closed-loop evolution profiles of Eq. (18) using 4 different ROMs with respect to the evolution profile from the higher-order discretization finite difference method.

where $a'_{s,i}(t) = [a_{s,i1}(t)\cdots a_{s,im_i}(t)]$ is a vector of the amplitudes of the first m_i eigenfunctions.

To present the effectiveness of empirical eigenfunctions in capturing the dominant trends that appear during closed-loop process evolution, we let the process evolve starting from a certain initial condition and under a constant input value, $u(t)=1$. Four different ROMs are presented and compared to show the ROM accuracy in the context of EMPC handling manipulated input and state constraints. Specifically, the following ROMs are considered:

1. ROM using 8 analytical sinusoidal/cosinusoidal eigenfunctions (e.g., 8 eigenfunctions for each PDE state; 16 eigenfunctions total).
2. ROM using 7 analytical sinusoidal/cosinusoidal eigenfunctions.
3. ROM using 4 empirical eigenfunctions.
4. ROM using 3 empirical eigenfunctions.

We compared the square of the L_2 norm, denoted as $||dX||_2$, to quantify the error of each of the reduced-order models. Specifically, we define $||dX||_2$ as

$$||dX||_2 = \sum_{i=1}^{2}\sum_{j=1}^{101}(x_{i,j}-\hat{x}_{i,j})^2, \quad i=1,2 \tag{38}$$

where $x_{i,j}$ and $\hat{x}_{i,j}$ are the state values of the i-th PDE at the j-th discrete points equally distributed along the spatial domain obtained from reduced order model and the finite difference method, respectively. The four different reduced-order models are compared with respect to the evolution profile from the higher-order discretization finite difference method (i.e., the two 101th-order set of ODEs obtained by discretizing, in space, the two parabolic PDEs of Eq. (18)) under the same initial condition and input value in Fig. 17. From the Fig. 17, comparing the L_2 norm between the ROM using 4 empirical eigenfunctions and the ROM using 8 analytical eigenfunctions, the ROM constructed from the empirical eigenfunctions is more accurate than the accuracy of the ROM constructed from analytical eigenfunctions with more modes. The average approximation error of each reduced-order model is at maximum of the order of 10^{-1}. Furthermore, we compared the computational efficiency under the above two different model reduction methods. The comparison of the computational time corresponding to these 4 different ROMs is given in Fig. 18. The ROM based on empirical eigenfunctions shows its advantage on the

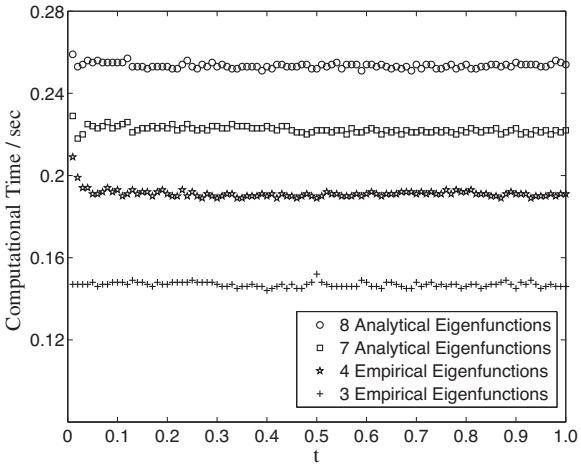

Fig. 18. Computational time profiles of Eq. (18) using 4 different ROMs.

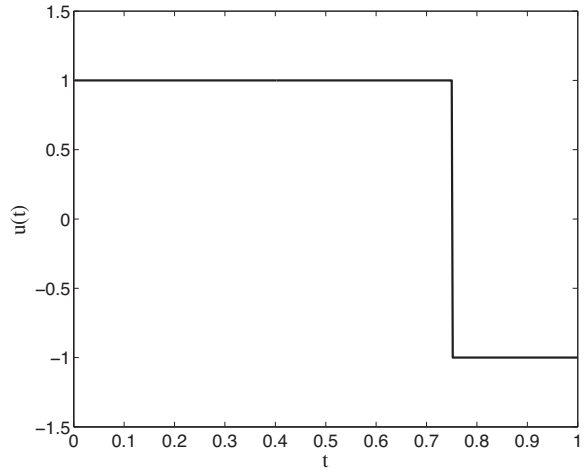

Fig. 19. Manipulated input profiles of the EMPC formulation of Eq. (39) using 4 different ROMs over one operation period (profiles are overlapping).

computational efficiency compared with the ROM based on the analytical sinusoidal/cosinusoidal eigenfunctions.

4.3. Implementation of EMPC

The implementations details of the EMPC are the same as for the output feedback case (see Section 3.3) except for two differences. First, the availability of the full state profile across the entire spatial domain is assumed at each sampling instance except for the third case study below, and second, the reduced-order model used in the EMPC is constructed using empirical eigenfunctions as basis functions.

4.3.1. Case 1: low-order EMPC system with input constraints only

In this set of simulations, we consider an EMPC formulation using the model of Eq. (37) and considering only input constraints which is of the form:

$$\max_{u\in S(\Delta)} \quad \frac{1}{N\Delta}\int_{t_k}^{t_{k+N}}\left(\int_0^1 r(z,\tau)dz\right)d\tau \tag{39a}$$

$$\text{s.t.} \quad \dot{\tilde{a}}_{s,i}(t) = A_{s,i}\tilde{a}_{s,i}(t) + F_{s,i}(\tilde{a}_s(t),0) + B_{s,i}u(t) \tag{39b}$$

$$\tilde{a}_{s,ij}(t_k) = (\overline{\phi}_{s,ij}(\cdot), \overline{x}_i(\cdot,t_k)), \quad j=1,\ldots,m_i, \quad i=1,2 \tag{39c}$$

$$-1 \le u(t) \le 1, \quad \forall t \in [t_k, t_{k+N}) \tag{39d}$$

$$u \in g(t_k) \tag{39e}$$

$$\tilde{a}_s'(t)P\tilde{a}_s(t) \le \overline{\rho} \tag{39f}$$

where the notation is similar to the notation of the EMPC formulations in the previous sections. The EMPC of Eq. (39) is applied with a prediction horizon $N=2$ and a sampling time $\Delta=0.01$.

The closed-loop behavior of the tubular reactor under an EMPC formulated with four different ROMs was considered: ROMs based on 3 and 4 empirical eigenfunctions and ROMs based on 7 and 8 analytical sinusoidal/cosinusoidal eigenfunctions. For $x(z,0)=0$, all of these 4 ROMs achieve the same manipulated input and closed-loop state profiles under the EMPC of Eq. (39) which are shown in Figs. 19–21, respectively. We emphasize here on the computational efficiency under the above two different methods. The comparison of the computational time corresponding to these 4 different situations is given in Fig. 22. The ROM based on empirical eigenfunctions shows its advantage on the computational efficiency compared with the ROM based on the analytical sinusoidal/cosinusoidal eigenfunctions.

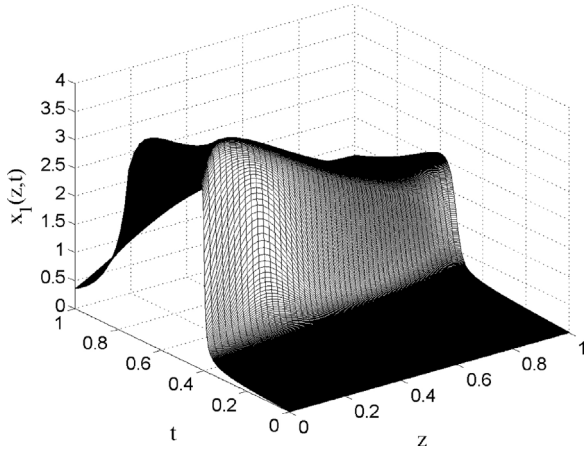

Fig. 20. Closed-loop profile of x_1 of the EMPC formulation of Eq. (39) using 4 different ROMs over one operation period (profiles are overlapping).

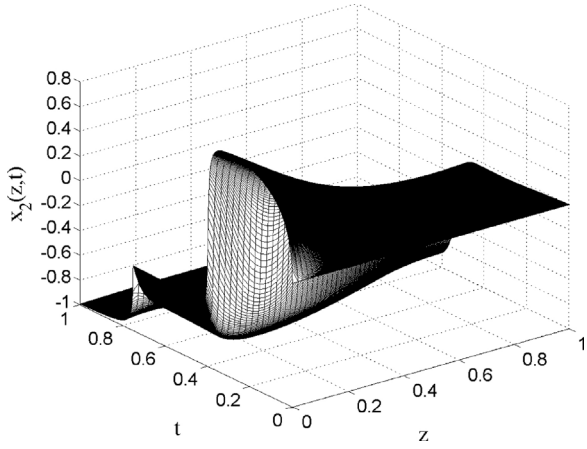

Fig. 21. Closed-loop profile of x_2 of the EMPC formulation of Eq. (39) using 4 different ROMs over one operation period (profiles are overlapping).

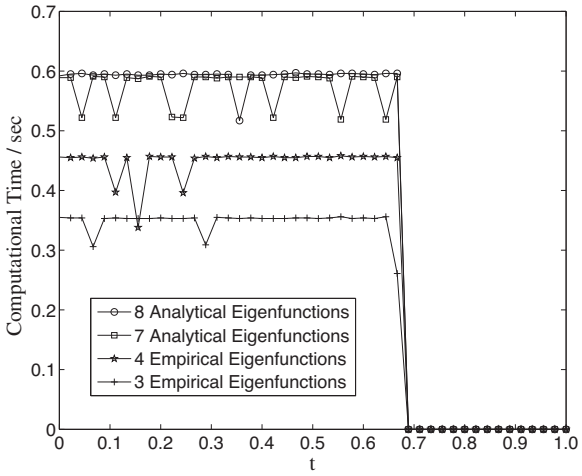

Fig. 22. Computational time profiles of the EMPC formulation of Eq. (39) using 4 different ROMs over one operation period.

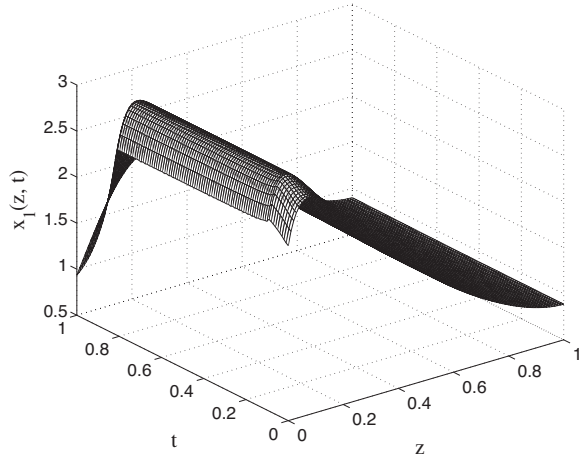

Fig. 23. Closed-loop profile of x_1 of EMPC formulation of Eq. (40) using the ROM based on 4 empirical eigenfunctions over one operation period.

4.3.2. Case 2: low-order EMPC system with state and input constraints

In this case, the state constraint of Eq. (28) into the EMPC formulation and thus, the EMPC formulation takes the form:

$$\max_{u\in S(\Delta)} \quad \frac{1}{N\Delta}\int_{t_k}^{t_{k+N}}\left(\int_0^1 r(z,\tau)dz\right)d\tau \tag{40a}$$

$$\text{s.t.} \quad \dot{\tilde{a}}_{s,i}(t) = A_{s,i}\tilde{a}_{s,i}(t) + F_{s,i}(\tilde{a}_s(t), 0) + B_{s,i}u(t) \tag{40b}$$

$$\tilde{a}_{s,ij}(t_k) = (\overline{\phi}_{s,ij}(\cdot),\ \overline{x}_i(\cdot, t_k)), \quad j = 1, \ldots, m_i, \quad i = 1, 2 \tag{40c}$$

$$-1 \le \sum_{j=1}^{m_i}\tilde{a}_{s,1j}(t)\phi_{1j}(z) \le 3 \tag{40d}$$

$$-1 \le u(t) \le 1, \quad \forall t \in [t_k, t_{k+N}) \tag{40e}$$

$$u \in g(t_k) \tag{40f}$$

$$\tilde{a}'(t)P\tilde{a}(t) \le \overline{\rho} \tag{40g}$$

We consider a prediction horizon $N=3$ and a sampling time $\Delta=0.01$. For this case, the initial condition is the steady-state of the system under uniform input distribution, $u=0.5$, as shown in the Figs. 23 and 24.

We compared the simulation results from the ROM based on 4 empirical eigenfunctions (i.e., $m_1=m_2=4$) and ROMs based on 8 and 12 sinusoidal/cosinusoidal eigenfunctions, respectively, for $x(z, 0)$ equal to the steady-state of the system under constant input value, $u(t)=0.8$. Figs. 23-24 show the closed-loop evolution of the states under the EMPC formulation of Eq. (40) from the ROM based on 4 empirical eigenfunctions. The manipulated input profiles for the above 3 different ROMs are given in Fig. 25, which have the same behavior as the ones in Case 1. For the input profile of ROM based on 4 empirical eigenfunctions in Fig. 25 (solid line), the chattering is caused by the over-estimated maximum temperature by the ROM in EMPC, which is also seen in Fig. 26 (solid line).

For this case study, we compared the integral of the reaction rate along the length of the reactor among the above 3 different ROMs and the case of the system under uniform in time distribution of the reactant material, i.e., $u(t)=0.5$, as shown in Fig. 27. From Fig. 27, for the cases of 3 different ROMs, the reaction rates under the EMPC significantly increase initially because of the second-order reaction rate dependence. The economic cost decrease since the

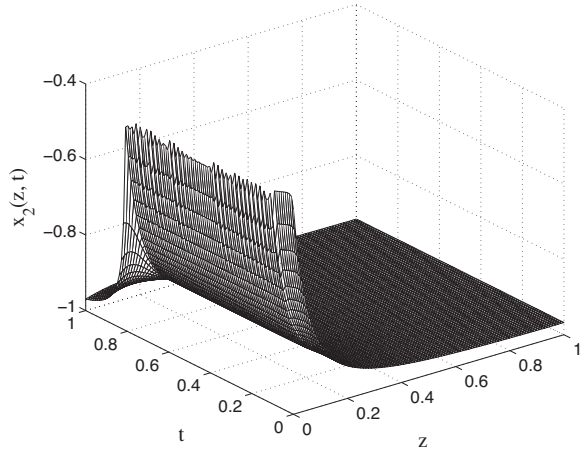

Fig. 24. Closed-loop profile of x_2 of EMPC formulation of Eq. (40) using the ROM based on 4 empirical eigenfunctions over one operation period.

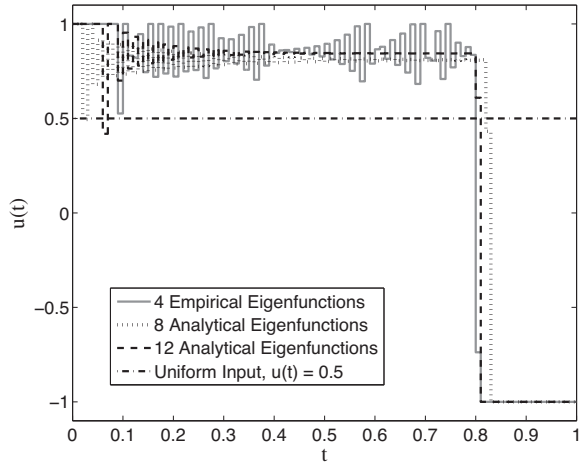

Fig. 25. Manipulated input profiles of the EMPC formulation of Eq. (40) using 3 different ROMs and uniform in time distribution of the reactant material profile over one operation period.

reactant material fed to the reactor decreases to satisfy the reactant material constraint. Over t_f, the total reaction rate from the system under the EMPC formulation from the ROM on the basis of 4 empirical eigenfunctions is 11.25% greater than that from the

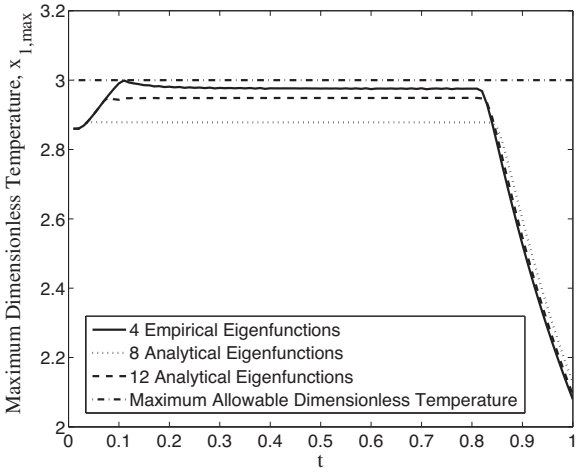

Fig. 26. Maximum temperature of x_1 profiles of the EMPC formulation of Eq. (40) using 3 different ROMs over one operation period.

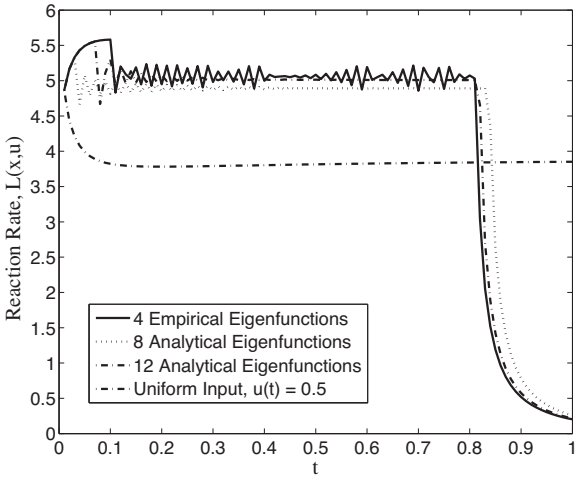

Fig. 27. The integral of the reaction rate along the length of the reactor of the tubular reactor under the EMPC formulation of Eq. (40) using 3 different ROMs and under uniform in time distribution of the reactant material over one operation period.

system under uniform in time distribution of the reactant material. The total economic cost of the ROM on the basis of 4 empirical eigenfunctions is 0.79% and 1.85% greater than that of the ROM on the basis of 8 and 12 analytical eigenfunctions, respectively. This can be explained from the point of view that the empirical eigenfunctions capture more information on the nonlinear terms and the input effect in the original PDE model which is not considered by the analytical eigenfunctions.

The comparison of the computational time corresponding to the EMPC systems based on the above 3 different ROMs is given in Fig. 28. The ROM based on 4 empirical eigenfunctions shows its advantage on the computational efficiency compared with the ROM based on both 8 and 12 analytical eigenfunctions.

4.3.3. Case 3: low-order output feedback EMPC system with state and input constraints

In this set of simulations, a low-order output feedback EMPC system (Eq. (35)) based on a ROM using empirical eigenfunctions is formulated and applied to the tubular reactor. The tubular reactor is initialized with $x(z, 0)$ equal to the steady-state of the system under constant input value, $u(t) = 0.6$. For the reactor, the low-order output feedback EMPC system based on the ROM using 4 empirical eigenfunctions is compared with the low-order output feedback

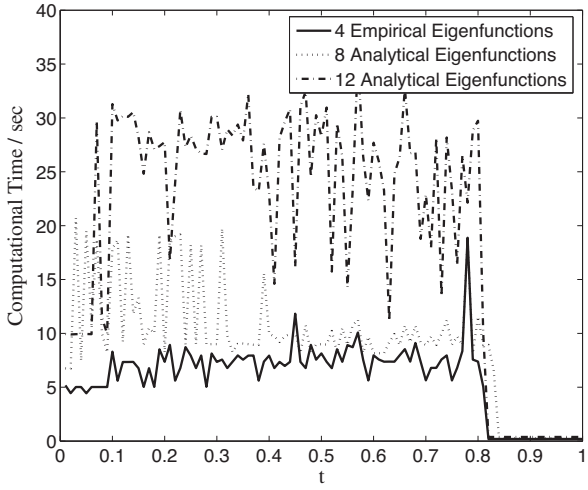

Fig. 28. Computational time profiles of the EMPC formulation of Eq. (40) using 3 different ROMs over one operation period.

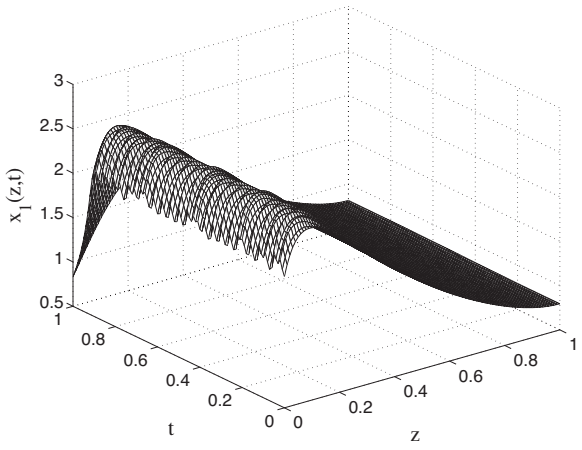

Fig. 29. Closed-loop profile of x_1 of EMPC formulation of Eq. (35) using the ROM based on 4 empirical eigenfunctions over one operation period.

EMPC system based on 11 slow modes only (i.e., $m_1 = m_2 = 11$). Additionally, the reactor under uniform in time distribution of the reactant material over $t_f = 1.0$ is also considered for comparison purposes.

We compared the simulation results from the low-order output feedback EMPCs using the ROM based on 4 empirical eigenfunctions (i.e., $m_1 = m_2 = 4$) and ROMs based on 11 sinusoidal/cosinusoidal eigenfunctions, respectively. Figs. 29-30 show the closed-loop evolution of the states under the EMPC formulation of Eq. (35) from the ROM based on 4 empirical eigenfunctions. The manipulated input profiles for the above 2 different ROMs are given in Fig. 31. For the input profile of ROM based on 4 empirical eigenfunctions in Fig. 31 (solid line), the chattering is caused by the over-estimated maximum temperature by the ROM in EMPC, which is also seen in Fig. 32 (solid line). Different from the simulation results in Section 4.3.2, the EMPC using the ROM based on 4 empirical eigenfunctions has higher amplitude of fluctuation on the input profile and also a much lower maximum temperature in the reactor. This difference results from the limited number of measurement points used with the EMPC using the ROM based on 4 empirical eigenfunctions (i.e., $p_1 = p_2 = m_1 = m_2 = 4$) compared to the EMPC using the ROM based on 11 analytical eigenfunctions (i.e., $p_1 = p_2 = m_1 = m_2 = 11$).

For this case study, we also compared the integral of the reaction rate along the length of the reactor among the above 2 different

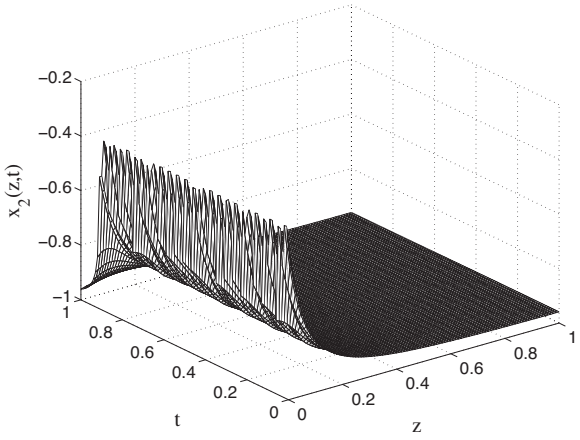

Fig. 30. Closed-loop profile of x_2 of EMPC formulation of Eq. (35) using the ROM based on 4 empirical eigenfunctions over one operation period.

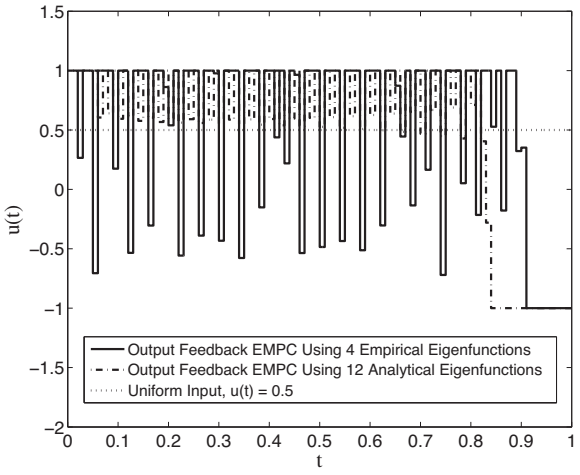

Fig. 31. Manipulated input profiles of the EMPC formulation of Eq. (35) using the ROM based on 4 empirical eigenfunctions and the ROM based on 11 analytical eigenfunctions and uniform in time distribution of the reactant material profile over one operation period.

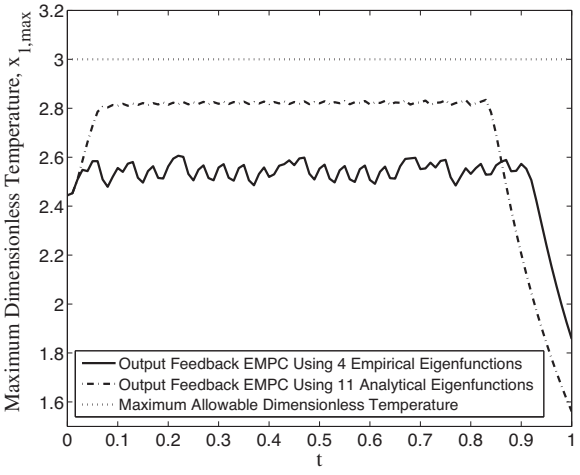

Fig. 32. Maximum temperature of x_1 profiles of the EMPC formulation of Eq. (35) using the ROM based on 4 empirical eigenfunctions and the ROM based on 11 analytical eigenfunctions and maximum allowable dimensionless temperature over one operation period.

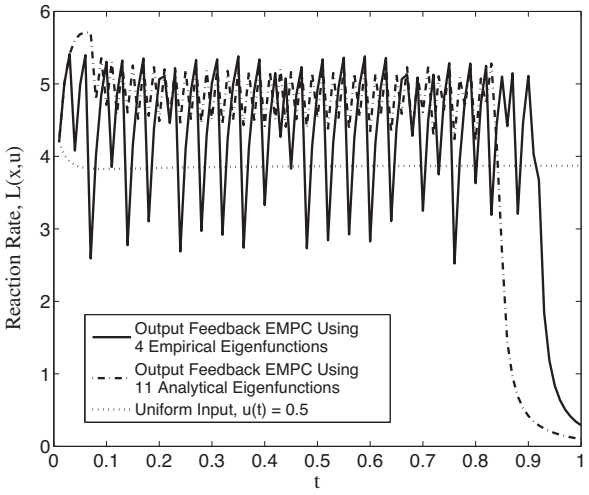

Fig. 33. The integral of the reaction rate along the length of the tubular reactor under the EMPC formulation of Eq. (35) using the ROM based on 4 empirical eigenfunctions and the ROM based on 11 analytical eigenfunctions and uniform in time distribution of the reactant material profile over one operation period.

ROMs and the case of the system under uniform in time distribution of the reactant material, i.e., $u(t) = 0.5$, as shown in Fig. 33. From Fig. 33, the total reaction rate over t_f from the system under the EMPC formulation from the ROM on the basis of 4 empirical eigenfunctions is still 9.45% greater than that from the system under uniform in time distribution of the reactant material and meanwhile, 1.46% less than that of the ROM on the basis of 11 analytical eigenfunctions.

5. Conclusions

In this work, two types of EMPC systems for quasi-linear PDE systems were presented: (1) an output feedback EMPC system and (2) an EMPC system formulated with a reduced-order model derived using empirical eigenfunctions as basis functions. The EMPC systems were applied to a tubular reactor of industrial importance. Through time-varying operation, the EMPC systems yielded improved closed-loop economic performance over steady-state operation. Additionally, constructing a ROM on the basis of historical data-based empirical eigenfunctions by applying Karhunen-Loève expansion demonstrated computational benefits over using analytical sinusoidal/cosinusoidal eigenfunctions as basis functions.

Acknowledgments

Financial support from the National Science Foundation and the Department of Energy is gratefully acknowledged.

References

[1] A. Armaou, P.D. Christofides, Dynamic optimization of dissipative PDE systems using nonlinear order reduction, Chemical Engineering Science 57 (2002) 5083–5114.
[2] J. Baker, P.D. Christofides, Finite-dimensional approximation and control of non-linear parabolic PDE systems, International Journal of Control 73 (2000) 439–456.
[3] M.J. Balas, Feedback control of linear diffusion processes, International Journal of Control 29 (1979) 523–534.
[4] S. Banerjee, J.V. Cole, K.F. Jensen, Nonlinear model reduction strategies for rapid thermal processing systems, IEEE Transactions on Semiconductor Manufacturing 11 (1998) 266–275.
[5] P.D. Christofides, Nonlinear and Robust Control of PDE Systems: Methods and Applications to Transport-Reaction Processes, Birkhäuser, Boston, 2001.

[6] P.D. Christofides, P. Daoutidis, Finite-dimensional control of parabolic PDE systems using approximate inertial manifolds, Journal of Mathematical Analysis and Applications 216 (1997) 398–420.
[7] M. Diehl, R. Amrit, J.B. Rawlings, A Lyapunov function for economic optimizing model predictive control, IEEE Transactions on Automatic Control 56 (2011) 703–707.
[8] S. Dubljevic, P.D. Christofides, Predictive output feedback control of parabolic partial differential equations (PDEs), Industrial & Engineering Chemistry Research 45 (2006) 8421–8429.
[9] S. Dubljevic, N.H. El-Farra, P. Mhaskar, P.D. Christofides, Predictive control of parabolic PDEs with state and control constraints, International Journal of Robust and Nonlinear Control 16 (2006) 749–772.
[10] S. Dubljevic, P. Mhaskar, N.H. El-Farra, P.D. Christofides, Predictive control of transport-reaction processes, Computers & Chemical Engineering 29 (2005) 2335–2345.
[11] C. Foias, M.S. Jolly, I.G. Kevrekidis, G.R. Sell, E.S. Titi, On the computation of inertial manifolds, Physics Letters A 131 (1988) 433–436.
[12] D. Georges, Infinite-dimensional nonlinear predictive controller design for open-channel hydraulic systems, in: Workshop on Irrigation Channels and Related Problems, vol. 4, Maiori, Salerno, Italy, 2009, pp. 267–285.
[13] M. Heidarinejad, J. Liu, P.D. Christofides, Economic model predictive control of nonlinear process systems using Lyapunov techniques, AIChE Journal 58 (2012) 855–870.
[14] M. Heidarinejad, J. Liu, P.D. Christofides, State-estimation-based economic model predictive control of nonlinear systems, Systems & Control Letters 61 (2012) 926–935.
[15] P. Holmes, J.L. Lumley, G. Berkooz, Turbulence, Coherent Structures, Dynamical Systems and Symmetry, Cambridge University Press, New York, New York, 1996.
[16] R. Huang, L.T. Biegler, E. Harinath, Robust stability of economically oriented infinite horizon NMPC that include cyclic processes, Journal of Process Control 22 (2012) 51–59.
[17] R. Huang, E. Harinath, L.T. Biegler, Lyapunov stability of economically oriented NMPC for cyclic processes, Journal of Process Control 21 (2011) 501–509.
[18] R. Huang, S.C. Patwardhan, L.T. Biegler, Robust stability of nonlinear model predictive control based on extended Kalman filter, Journal of Process Control 22 (2012) 82–89.
[19] K. Ito, K. Kunisch, Receding horizon optimal control for infinite dimensional systems, ESAIM: Control, Optimisation and Calculus of Variations 8 (2002) 741–760.
[20] L. Lao, M. Ellis, P.D. Christofides, Economic model predictive control of transport-reaction processes, Industrial & Engineering Chemistry Research (2014), http://dx.doi.org/10.1021/ie401016a, in press.
[21] T.V. Pham, D. Georges, G. Besançon, Receding horizon boundary control of nonlinear conservation laws with shock avoidance, Automatica 48 (2012) 2244–2251.
[22] S. Pitchaiah, A. Armaou, Output feedback control of distributed parameter systems using adaptive proper orthogonal decomposition, Industrial & Engineering Chemistry Research 49 (2010) 10496–10509.
[23] W.H. Ray, Advanced Process Control, McGraw-Hill, New York, New York, 1981.
[24] H. Shang, J.F. Forbes, M. Guay, Model predictive control for quasilinear hyperbolic distributed parameter systems, Industrial & Engineering Chemistry Research 43 (2004) 2140–2149.
[25] H. Shang, J.F. Forbes, M. Guay, Computationally efficient model predictive control for convection dominated parabolic systems, Journal of Process Control 17 (2007) 379–386.
[26] L. Sirovich, Turbulence and the dynamics of coherent structures, I – Coherent structures. II – Symmetries and transformations. III – Dynamics and scaling, Quarterly of Applied Mathematics 45 (1987) 561–590.
[27] A. Theodoropoulou, R.A. Adomaitis, E. Zafiriou, Model reduction for optimization of rapid thermal chemical vapor deposition systems, IEEE Transactions on Semiconductor Manufacturing 11 (1998) 85–98.
[28] A. Varshney, S. Pitchaiah, A. Armaou, Feedback control of dissipative PDE systems using adaptive model reduction, AIChE Journal 55 (2009) 906–918.
[29] A. Wächter, L.T. Biegler, On the implementation of an interior-point filter line-search algorithm for large-scale nonlinear programming, Mathematical Programming 106 (2006) 25–57.